ELSEVIER

Polymer 42 (2001) 3475–3487

polymer

www.elsevier.nl/locate/polymer

Effects of sample preparation method on mixing and phase separation in binary polymer blends

P. Rojanapitayakorn[a], S. Thongyai[a], J.S. Higgins[b,*], N. Clarke[c]

[a]*Department of Chemical Engineering, Chulalongkorn University, Phayathai Road, Bangkok 10330, Thailand*
[b]*Department of Chemical Engineering and Chemical Technology, Imperial College of Science, Technology and Medicine, Prince Consort Road, London SW7 2BY, UK*
[c]*Department of Chemistry, University Science Laboratories, University of Durham, South Road, Durham DH1 3LE, UK*

Received 12 June 2000; received in revised form 29 September 2000; accepted 20 October 2000

Abstract

Detailed studies of effects of sample preparation method on the kinetics of phase separation in a blend of polystyrene-*co*-maleic anhydride (SMA) with a commercial sample of polymethyl methacrylate containing ethyl acrylate as co-monomer (PMMAe) have been performed using light scattering techniques. Two preparation methods, viz. solution casting and melt mixing in a mini twin screw extruder were employed in this work. The blend, which shows lower critical solution temperature (LCST) behaviour, exhibits spinodal and binodal curves at higher temperatures in the case of solution casting than those from melt mixed samples. The relative values of the Cahn–Hilliard growth rate, $R(q)$, obtained from the two preparation methods depend on blend concentration, $R(q)$ being faster for solution cast samples at some concentrations and slower at others. Comparison of the data with recent theoretical developments for entangled polymer blends is reported.

Keywords: Polymer blend; Phase separation; Sample preparation method

1. Introduction

During the past few decades polymer miscibility and the kinetics of phase separation have been extensively investigated. Several sample preparation methods have been employed in these studies but the solution casting method has generally dominated [1–9]. A number of parameters have been found to affect the miscibility and phase boundary conditions, for example, film thickness, substrates, types of solvent, evaporation rate of solvent, etc. [2–10]. Since the solvent plays an important role as has been reported in a number of papers [7–10], it is interesting to observe the thermodynamics and kinetics of phase behaviour in blends, which are obtained without the use of solvents by the method widely used for commercial samples, i.e. melt mixing. An early study by Gaurab et al. [9] using a differential scanning calorimeter (DSC) on blends, which were prepared by 2 different techniques, viz. solution casting and melt mixing from co-precipitated samples, showed that the latter provided the most compatible blends. Other measurements by Thongyai [11] on tetra methyl-bis-phenyl-A polycarbonate with polystyrene (TMPC/PS) and Manda [12,13] on poly (styrene-*co*-maleic anhydride) with polymethyl methacrylate (SMA/PMMAe) using solution cast and melt mixing methods showed that to employ a direct melt mixing method in the blend can lower the cloud point curve. They suggested that the cloud point curve of the melt mixed samples might coincide with the binodal curve because the large number of heterogeneties in such samples provide multiple nucleating sites for the nucleation and growth mechanism once the sample is inside the metastable region. However, to date no spinodal curve of melt mixed samples has been reported.

Blends of PMMA and SMA are becoming of interest nowadays owing to the high glass transition temperature (T_g) of styrene maleic anhydride copolymer, which can elevate the processing temperature in blends. The miscibility of this blend has been previously investigated by several groups. Previous work by Paul et al. [14] on the PMMA/SMA blend, using various maleic anhydride contents, in DSC measurements showed that the miscibility of the blend was dependent on MA content. Using pure polyethyl methacrylate (PEMA) instead of pure PMMA lowered the cloud point curve. Light scattering experiments carried out

* Corresponding author. Tel.: +44-207-594-5565; fax: +44-207-594-5638.
E-mail address: j.higgins@ic.ac.uk (J.S. Higgins).

0032-3861/01/$ - see front matter
PII: S0032-3861(00)00783-7

on a similar blend but with a commercial PMMAe sample (with ethyl acrylate co-monomer) by Manda et al. [12,13] showed similar results to the PMMA system but with a slightly lower cloud point due to the co-monomer. Feng et al. [15] investigated the mechanism for miscibility of SMA/PMMA blends using NMR, FT-IR and DSC. It was suggested that a strong intermolecular interaction between the phenyl groups in SMA and the carbonyl groups in PMMA resulted in the miscibility at a molecular level. The strength of the interaction depends on the compositions of the blends. The effect of shear mixing and de-mixing on blends using the commercial PMMAe have been reported by Aelmans et al. [16] and Chopra et al. [17].

During isothermal heating of the blend inside the spinodal region, one surprising phenomenon, which is still ambiguous, has been detected — a so-called delay time. The phenomenon refers to a time period after a jump to a temperature inside the spinodal, during which no apparent phase separation occurs — at least as observed by light scattering. Relatively few studies so far have mentioned this behaviour, among which we cite Refs. [11–13,18–21]. Previous work on the polystrene/poly(vinyl methyl ether) (PS/PVME) blend system from Bank et al. [18] using an optical microscope showed that the delay times decreased as temperature increased. A theoretical approach developed by Binder [19] was used to describe the interaction between the rheological relaxation mechanisms of the polymers and the concentration fluctuations. However, there was no comparison between the theory and experimental data. The model, which was subsequently elaborated by Clarke et al. [20], showed that entanglement networks were the key factor causing delay times. This proposition was supported by light scattering experiments on ultra high molecular weight polystyrene–polyvinyl methyl ether (PS/PVME) blends. It was found that delays were observed for polystyrene of very high molecular weight. A study by Thongyai [11] on TMPC/PS blends using light scattering suggested that the delay time phenomena could be observed in this system only for certain compositions, notably those with a high percentage of TMPC which is the high T_g component. Experimental work by Manda et al. [12,13] showed that delay times can also be detected in the SMA/PMMAe blend system. Shear-induced phase separation in PS/PVME blends studied by Gerard et al. [21] manifested that not only can delay times be observed in thermally induced phase separation, but also in shear-induced phase separation. Most experiments however have been performed only in the low q-range scale, accessible in light scattering experiments and restricted to observing phase separation larger than a few hundred nanometres. Data from the high-q range accessible in small angle X-ray or neutron scattering experiments would clarify the question as to whether any early phase separation is taking place during this delay time in a small size scale off range in light scattering.

This paper reports the evidence for effects of sample preparation methods on the mixing and phase separation of SMA/PMMAe blends. The spinodal curves of melt mixed samples were measured and compared with the solution cast samples. The kinetics of phase separation of both solution cast and melt mixed samples were explored in some detail. The delay time, which is in fact the subject of ongoing research, also shows the effects of preparation method. In the final part of this paper a preliminary analysis of the delay times using the model proposed by Clarke et al. [20] is reported.

2. Theoretical background

The Flory–Huggins lattice model [22] describes the free energy of mixing (F_{FH}) for two polymer molecules (A and B) as,

$$F_{FH}/k_BT = \frac{\phi}{N_A}\ln\phi + \frac{(1-\phi)}{N_B}\ln(1-\phi) + \chi\phi(1-\phi) \tag{1}$$

where k_B is Boltzmann's constant, ϕ the volume fraction of polymer A, N_A, N_B are the degree of polymerisation of A and B, and χ the Flory–Huggins interaction parameter.

In order to account for the effect of concentration gradients on the free energy of polymer blends, de Gennes [23] later introduced an additional term into the Flory–Huggins free energy,

$$F_{FH-dG}/k_BT = \frac{\phi}{N_A}\ln\phi + \frac{(1-\phi)}{N_B}\ln(1-\phi) + \chi\phi(1-\phi) + \kappa(\nabla\phi)^2 \tag{2}$$

where κ is a measure of the interfacial energy, determined from the random phase approximation as,

$$\kappa = \frac{b^2}{36\phi(1-\phi)} \tag{3}$$

where b is the Kuhn statistical segment length and for simplicity, we assume an average b value for the two polymers.

The usual starting point for considering the dynamics of concentration fluctuations and the early stages of phase separation is the linearised Cahn–Hilliard equation of motion for $\delta\phi(\mathbf{r},t) = \phi(\mathbf{r},t) - \phi_0$, the difference in the local concentration from the average, ϕ_0. The Cahn–Hilliard equation is,

$$\frac{\partial\,\delta\phi_q(t)}{\partial t} = -q^2M(q)\frac{\partial F[\delta\phi_q(t)]}{\partial\,\delta\phi_q(t)} \tag{4}$$

where $M(q)$ is a mobility and the Fourier transform of $\delta\phi(\mathbf{r},t)$ can be defined as,

$$\delta\phi_q(t) = \frac{1}{(2\pi)^{3/2}}\int d\mathbf{r}\,\delta\phi(\mathbf{r},t)\exp\{-i\mathbf{q}\cdot\mathbf{r}\} \tag{5}$$

and $F[\delta\phi_q(t)]$ is the Fourier transformed Flory–Huggins–

deGennes free energy, which can be written as,

$$F_{\mathrm{FH-dG}}[\delta\phi_q(t)] = \sum_q [\chi_s - \chi + \kappa q^2]\,\delta\phi_q^2 \tag{6}$$

where χ_s is the value of the interaction parameter on the spinodal curve. From Eqs. (5) and (6), the scattering function $S_q(t)$, defined as,

$$S_q(t) = \langle|\delta\phi_q(t)|^2\rangle \tag{7}$$

is found to be,

$$S_q(t) = S_q(0)\exp\{2R(q)t\} \tag{8}$$

where $R(q)$ is the q dependent growth rate of concentration fluctuations, given by,

$$R(q) = -2q^2M[\chi_s - \chi + \kappa q^2] \tag{9}$$

Generally, the growth or decay with time depends on whether $R(q)$ is positive of negative. In the one phase region, and even in the metastable region, $R(q)$ is always negative, consequently concentration fluctuations always decay. On the other hand, in the unstable region where the blend undergoes spinodal decomposition, $R(q)$ is positive for q less than some critical value, q_c,

$$q_c = \sqrt{(\chi - \chi_s)/\kappa} \tag{10}$$

Hence, fluctuations with such wave vectors grow following a jump into the 2-phase region, with the fastest growing wave vector given by,

$$q_m = \sqrt{(\chi - \chi_s)/2\kappa} \tag{11}$$

Inserting the maximum wave vector into Eq. (9), we obtain the maximum relative growth rate $R(q_m)$:

$$R(q_m) = \frac{M[\chi - \chi_s]^2}{2\kappa} \tag{12}$$

3. Polymer entanglements

In order to take into consideration the effect of entanglement in high molecular weight polymer systems, Clarke et al. [20,24] introduced a transient elastic energy term into the Cahn–Hilliard equation. There are two cases of interest: A–B entanglements, in which both components are mutually entangled, and A–A entanglements which are dominated by one component. In order to proceed, we assume herein that the rates associated with concentration fluctuation dynamics are much slower than the rheological rates, i.e. $R_T \ll R_{CO}, R_V$. This assumption will be valid for all but very highly entangled chains, and in general corresponds to blends in which the component relaxation times are of the order of 1 sec or less. Under these conditions, the resultant scattering function may be written as,

$$S_q(t)/S_q(0) \approx A_1\exp\{-(R_V + R_{CO})t\} + (1 - A_1)\exp\left\{-\left(\frac{R_T R_V}{R_V + R_{CO}}\right)t\right\} \tag{13}$$

where $R_T = 2q^2M[\chi_s - \chi + \kappa q^2]$, $R_{CO} = 2C_o(q)Mq^2$, $R_V = 1/\tau$, and $A_1 = R_{CO}/(R_V + R_T)$. The magnitude of the effect of the elastic energy is determined by the form of the parameter $C_o(q)$, which for A–B entanglements is written in the form,

$$C_o(q) = \frac{36}{N_e^2 b^2 q^2} \tag{14}$$

where N_e is the number of monomers between entanglement points. For A–A type entanglements, the elastic energy arises due to swelling of the entanglement network, and

$$C_o(q) = \frac{3\phi_A}{N_e} \tag{15}$$

The magnitude of rate R_T is identical to the relaxation growth rate, $R(q)$ of the Cahn–Hilliard equation. It represents the thermodynamic mode, whereas the other two rates, namely R_{CO} and R_V give rise to additional viscoelastic modes. The time τ, which appears in R_V, is the relaxation time of a chain, which for highly entangled polymers is given by the tube model [25] as,

$$\tau = \frac{\zeta}{\pi^2 k_B T}\frac{b^4}{a^2}N^3 \tag{16}$$

where ζ is the friction coefficient of a monomer and a is the step length of the primitive chain which is of the order of $N_e^{1/2}b$.

The summation of R_V and R_{CO} in the first term of Eq. (13) is always positive, whereas the product of R_T and R_V in the second term on the right-hand side term can be either positive or negative depending on R_T. Hence, the first term represents a decaying mode, while the second one represents a growing mode.

We can use Eq. (13) to derive an approximate relation between the delay time before growth of fluctuations and the eventual growth rate. If we first assume that the delay time τ_d is given by the relation, $S_q(\tau_d) \approx S_q(0)$, and that after that time the decaying term is negligible, we have,

$$(1 - A_1)\exp\{-R_2\tau_d\} \approx 1 \tag{17}$$

where R_2 is the observed modified growth rate, which includes the slowing down due to viscoelasticity. From Eqs. (13) and (17) we find,

$$|R_2\tau_d| \approx \ln(1 + 2C_o(q)M\tau q^2) \tag{18}$$

The mobility of concentration fluctuations M may be written as,

$$M = \frac{k_B T N_e}{3\zeta N} \tag{19}$$

Table 1
The characteristics of the polymers used in this study

Polymer	M_w	M_w/M_n	T_g (°C)	Density (g/cm^3)[a]
SMA	80,000[b]	2–2.5	175.7	1.182
PMMAe	120,000[c]	2	100.4	1.185

[a] Determined by Pycnometer Micromeritics AccuPyc 1330.
[b] Provided by DSM.
[c] Determined by Gel Permeation Chromatography analysis using PS standards.

so that,

$$M\tau \approx \frac{N^2 b^2}{3\pi^2} \tag{20}$$

which is independent of the monomeric friction coefficient.

As C_o relies on types of entanglement dominating the system, it can be seen that Eq. (17) depends on the model chosen. If the A–B entanglement model is chosen, it results in the product of delay time and the relative growth rate being independent of q,

$$|R_2\tau_d| \approx \ln\left(1 + \frac{24N^2}{\pi^2 N_e^2}\right) \tag{21}$$

On the other hand, if we assume that PMMA dominates the rheological properties of the system, i.e. the system behaves as an A–A entanglement network, Eq. (18) can be written as,

$$|R_2\tau_d| \approx \ln\left(1 + \frac{2\phi_{PMMA}N^2 b^2}{\pi^2 N_e} q^2\right) \tag{22}$$

We can use Eqs. (21) and (22) to test whether our delay times and growth rates are consistent with known rheological data. The principal advantage of Eqs. (21) and (22) is that we have factored out the effect of the quench depth.

4. Experiment

4.1. Materials

The random copolymer of styrene maleic anhydride (SMA), containing 32% by weight of maleic anhydride (MA), was kindly provided by DSM. Owing to its hygroscopic nature it was stored in a dry atmosphere and heated prior to use. The samples were dried immediately prior to use by heating in a vacuum oven at 120°C for 4 h. Details of the SMA polymerisation can be found in the relevant publications of Bauruach et al. [26], Wang [27], Klumperman et al. [28] and Tacx et al. [29]. The commercial grade of poly(methyl methacrylate) (PMMAe), containing 10 wt% copolymerised ethyl acrylate co-monomer was supplied by ICI (UK). It comprises ca. 0.75 wt% of lubricating agent, 0.02 wt% UV stabiliser, and 0.1 wt% heat stabiliser. The commercial PMMAe polymer was chosen for these studies because blending SMA with PMMA gives high cloud point curves [12] and samples are very vulnerable to thermal degradation during the phase separation experiments. Preliminary work on the pure PMMA material showed that it is difficult to detect phase boundaries at slow heating rates because of degradation. At the high temperatures used to follow spinodal decomposition inside the phase boundary, degradation became prohibitive. Using the commercial PMMAe grade both lowers the phase boundary and greatly increases thermal stability. Characteristics of both polymers have been shown in Table 1.

5. Sample preparation

5.1. Solution casting

Solution cast specimens were prepared by mixing 10% (w/v) different weight compositions of blends in methyl ethyl ketone. The solution was coated onto the top of 16 mm diameter glass cover slips and kept at room temperature for 1 day. It was further dried in a vacuum oven in which the temperature was raised gradually until at least 20°C above the glass transition temperatures of the blend (approximately 2 weeks) and constant weight was reached.

5.2. Melt mixing

Both polymers were mixed using a PRISM twin screw extruder at temperature between 200–210°C and compressed into thin film (approximately 0.1–0.15 mm) at 190°C for light scattering experiments using a hot press. It should be noted that the temperatures used in the extruder here fall inside the phase separation regime hence two-phase cloudy samples were produced. It is therefore necessary to anneal them inside the miscible regime prior to use. The beads were heated at a temperature 20 degrees above their glass transition temperatures overnight after which they became perfectly transparent.

6. Experimental techniques

6.1. Differential scanning calorimeter

Samples weighing between 10 and 15 mg were placed on the aluminium pan and heated at the rate of 20°C/min from room temperature to approximately 20 degrees beyond the end of the T_g transition using a Pyris 1 Differential Scanning Calorimeter. Samples were then quenched to room temperature, held for 5 min and heated again at the same rate. The mid point of the specific heat change is defined as the glass transition temperature, T_g. The second run T_g was used in order to avoid the effect of thermal history.

6.2. Fourier transform infrared spectrometer

FT-IR experiments using a FTIR-1760 Perkin–Elmer

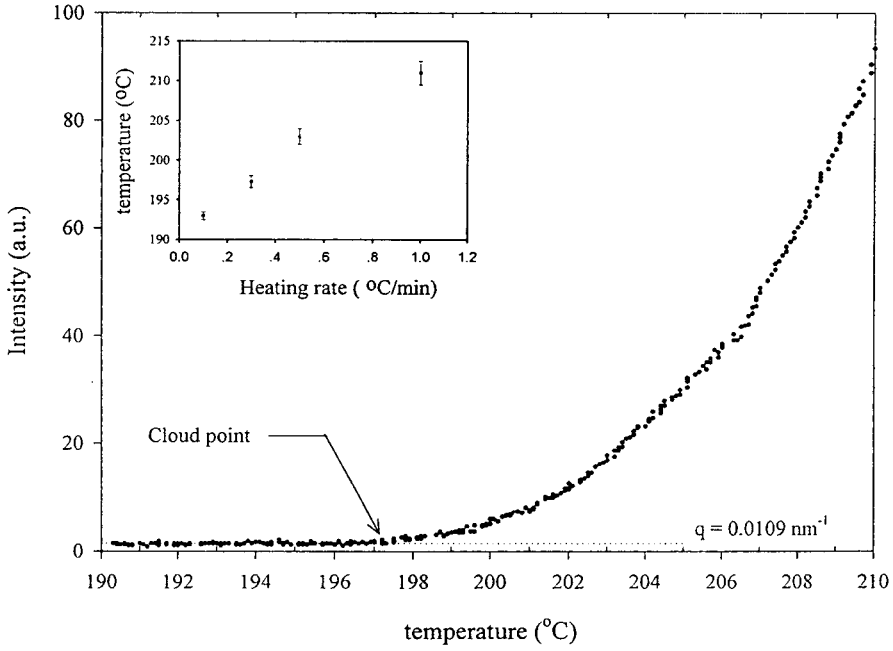

Fig. 1. A plot of intensity against temperature for melt mixed SMA/PMMAe (20/80) blend at the heating rate of 0.3°C/min. The cloud point temperature can be obtained from the rising temperature, as seen in the figure, it is approximately 197°C. Inset: the heating rate dependence of cloud point temperatures.

spectrometer were carried out to observe interactions and the approximate concentrations of the blends. Measurements were taken at 8 cm^{-1} resolution. Samples were ground and mixed with potassium bromide using a small vibration ball mill. They were then pressed into cylindrical plates and mounted on a holder for subsequent measurement of the spectra. Comparing areas under the phenyl peaks of blends with that of pure SMA, allowed approximate concentrations of the blends to be obtained.

6.3. Light scattering

Kinetic experiments were performed using a light scattering apparatus which was built in our laboratory. Details of

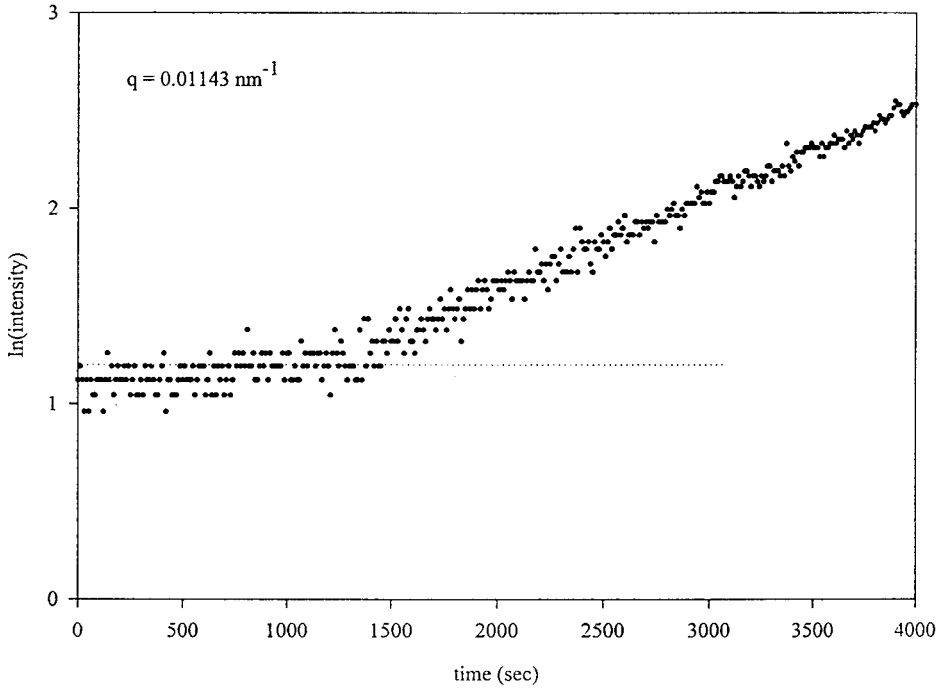

Fig. 2. A plot of ln(intensity) against time for melt mixed SMA/PMMAe (20/80) blends, obtained from a temperature jump experiment at 205°C. As seen in this figure, the delay time is approximately 1500 s.

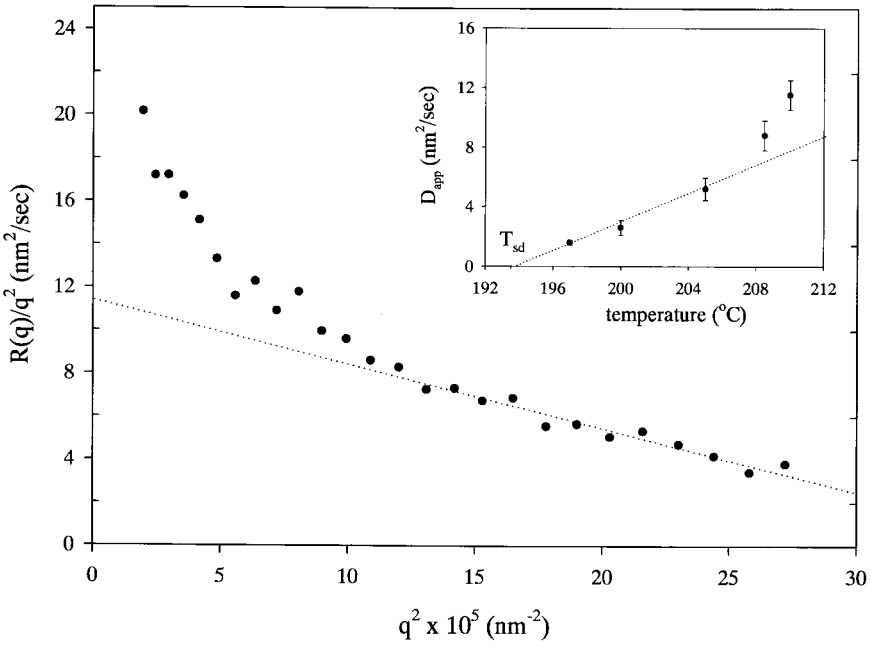

Fig. 3. A plot of $R(q)/q^2$ against q^2 for melt mixed SMA/PMMAe (40/60) blends, obtained from a temperature jump experiment at 210°C. The range of q^2 between 0.00015 and 0.00025 nm^{-2} was chosen to find D_{app}. Inset: the spinodal temperature can be obtained from extrapolating D_{app} to zero, as seen in this figure it is approximately 194°C.

the design can be seen elsewhere [11,12,30,31]. A heated sample block holds the blend on which a laser beam impinges. Scattered transmitted light is detected on a photodiode array covering an arc of 60 degrees. The wave vector, q, is then given by $(4n\pi/\lambda)\sin(\theta/2)$, where λ is the wavelength of the laser = 632.8 nm, θ is the scattering angle and n is the refractive index of the blend.

Two different methods were employed using the light scattering apparatus, viz. a cloud point experiment, and a temperature jump experiment. In the former case, a number of dry films of each composition were heated at different heating rates. The point at which the scattered intensities start to increase is defined as the cloud point as shown in Fig. 1. Since cloud point values depend on the rate at which phase separation in the sample responds to the temperature changes, as a rule, the lower the heating rate the lower the cloud point value. Extrapolating heating rate to zero is then used to obtain a value close to the true cloud point. It has recently been shown that for some systems there is a distinct change in the slope of the curve of cloud point with heating rate [12,13,31], and it has been suggested that two mechanisms may be being detected. The faster process, which shows up at the higher heating rates could then be spinodal decomposition, while the slow response could be nucleation and growth. If this is the case, then extrapolation of the two lines to zero heating rate will give an indication of both the spinodal and binodal temperatures of the blend. For our cloud point measurement, several heating rates (0.1, 0.3, 0.5, 1°C/min) were chosen. No change in slope was observed and moreover when the angular dependence was examined, spinodal peaks were observed for all experiments, confirming that spinodal decomposition was occurring. Extrapolation to zero heating rate as shown in the inset in Fig. 1 was used to obtain the cloud point.

The second set of experiments was designed to determine the spinodal temperatures, by following the spinodal decomposition process after a temperature jump inside the phase boundary. Homogeneous blends were annealed first at 160°C (i.e. above their T_g and below the cloud point temperature) for 10 min and then transferred quickly into the sample holder, which was pre-heated to the desired temperature inside the phase boundary. The rate of change of intensity with time (after any delay time, as described in results Section 6 below) on each of the photodiodes provides the Cahn–Hilliard growth rate $R(q)$ as seen in Fig. 2. Eq. (9) leads to a definition of the apparent diffusion coefficient, $D_{app} = [R(q)/q^2]_{q\to 0}$. In other words, the D_{app} can be obtained from the intercept of a plot of $R(q)/q^2$ versus q^2 as shown in Fig. 3. However it should be noted that the data in Fig. 3 are not linear. Similar effects, frequently observed in the literature [12,13,19,20,31,32], have been attributed to thermal fluctuations or to polymer relaxation. We chose to extrapolate the high q-data range, as this is less likely to be contaminated by any initial inhomogeneities in the sample such as dust or unmixed polymers. It can be seen from Eq. (9) that D_{app} tends to zero at the spinodal temperature ($\chi = \chi_s$). Spinodal points therefore can be obtained by extrapolating the apparent diffusion coefficient to zero as shown in the inset in Fig. 3.

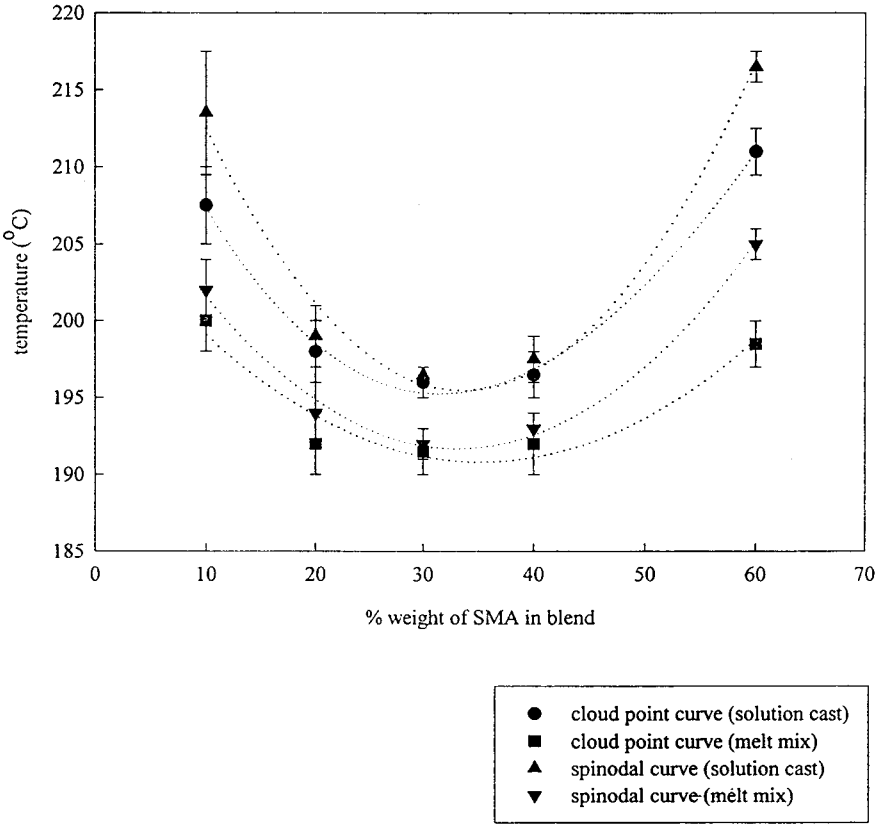

Fig. 4. Phase diagrams of SMA/PMMAe blends prepared by solution cast and melt mixed method, determined by the light scattering technique. The cloud points were obtained from zero heating rate method using heating rate of 0.1, 0.3, 0.5°C/min. The spinodal points were determined by extrapolating D_{app} to zero.

7. Result and discussion

7.1. Phase behaviour

Cloud point and spinodal curves of melt mixed and solution cast blends are shown in Fig. 4. The blends, which first are clear, become cloudy after heating indicating lower critical solution temperature (LCST) behaviour. When considering cloud point measurements, it should be noted that the existence of delay times can result in the observed temperature overshooting the real cloud point temperature. Hence, the lower the heating rate data are likely to lie closer to the real cloud point temperature.

As seen in Fig. 4, spinodal curves from samples prepared by both methods are close to their cloud point curves. Hence, the cloud point curve obtained in this work are likely to represent the spinodal curve, especially at compositions not far from the critical values which lie between 20–40 wt% of SMA in blends.

Concerning the EA content in our PMMAe, Paul et al. [14] pointed out that phase boundaries of the pure PEMA are very similar to the pure PMMA, with a slightly lower curve for PEMA. Manda et al. [12,13], and Chopra et al. [17], who both used commercial PMMAe, but with slightly different EA contents reported very similar phase diagrams to those in Fig. 4, the differences being well within the variation to be expected from the difference of additive contents, material sources, and measurement methods.

As seen in Fig. 4, although there is a considerable scatter in the data, there does appear to be a real shift of about 5°C between the values for the melt mixed and solution cast samples. The melt mixed samples appear to exhibit systematically lower spinodal and cloud point curves than solution cast samples. This indicates that at the same composition if both samples are heated simultaneously, the melt mix samples will become cloudy signalling demixing first. This may be as a result of the solution cast method allowing polymers to mix completely at a molecular level and facilitating specific interactions between them. It subsequently requires much more energy for the solution cast blend to break the molecular interactions before phase separation proceeds. This argument gains some supports from FT-IR experiments. The IR spectra of the blends, prepared by the two methods showed some evidence of the shifts in the phenyl group vibration for styrene and the carbonyl group motion in PMMA, as reported by Feng et al. [15], and in some samples there is clearly a larger effect in the solution cast than in the melt mixed samples. This may indicate differences in the strength of the interactions as been reported by Coleman et al. [33].

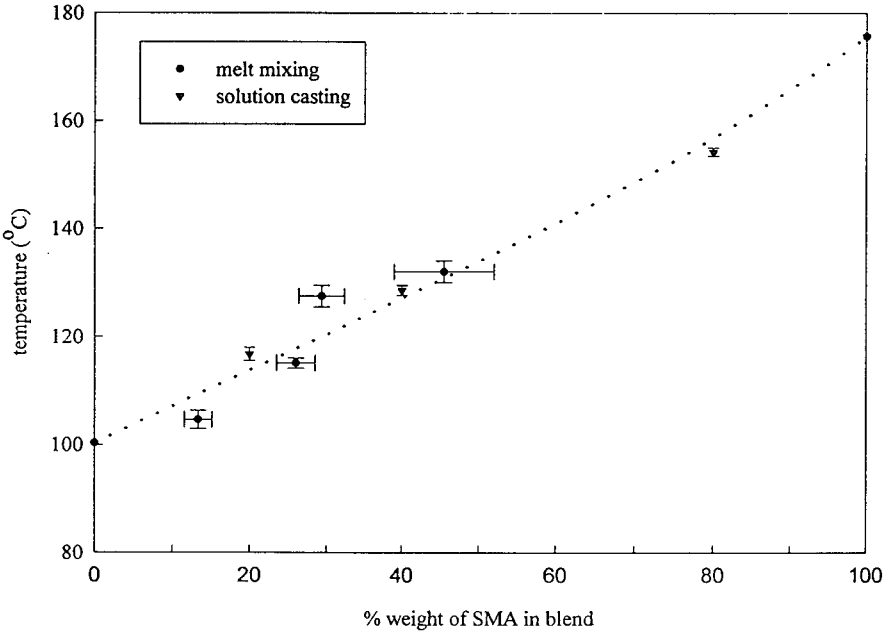

Fig. 5. Plots of glass transition temperature of SMA/PMMAe blends. The dotted line illustrates the Gordon–Taylor–Kwei equation using $k = 1.75$, $\alpha = 25$ K.

7.2. Glass transition temperature (T_g)

A single T_g, intermediate between those of the two components, was observed for all compositions of the as prepared samples demonstrating the miscibility of these two polymers. Experimental results obtained from DSC show only very minor differences between T_g of solution cast and melt mixed samples. These fall within the experimental errors, and confirm that all solvent in the solution cast blends has been removed.

Since all compositions show a positive deviation from the Fox equation [34], the Gordon–Taylor–Kwei empirical equation [17], which takes into account the influence of interactions was employed in this work.

$$T_g = \frac{X_1 T_{g1} + kX_2 T_{g^2}}{X_1 + kX_2} + \alpha X_1 X_2 \tag{23}$$

where the first term on the right-hand side of Eq. (23) is identical with the widely used Gordon–Taylor expression [35], and the second term represents the effect of polymer–polymer interaction, e.g. hydrogen bonding. Using $k \approx T_{g1}/T_{g2} = 1.75$, $\alpha = 25$ K, Eq. (23) provides a reasonable fit to the data as seen in Fig. 5. Such a fit is typical of systems with specific interactions between the component polymers.

7.3. Growth rate (R(q))

The growth rates, $R(q)$, are shown in Fig. 6a and b as a function of q for four compositions and the two preparation techniques, phase separated at similar temperatures. Comparing melt mixed and solution cast blends at the same temperature, since the former is deeper inside spinodal regime than the latter (see Fig. 4), it might be expected that the melt mix blend should phase separate faster than the solution cast blend due to the larger quench depth. However, a much more complex effect was observed in practice. It was found that $R(q)$ obtained from the melt mix method for SMA/PMMAe (10/90) is higher than from the solution cast method, while for other compositions the opposite effect was observed. For the SMA/PMMAe (30/70) blend, which is believed to be at the critical composition (as seen in Fig. 4), the solution cast blend phase separates much faster than the melt mix blend does, whereas only minor difference occurred for 20/80 and 40/60 compositions. This may imply complex differences in the thermodynamic behaviour of the blends. A variation with both temperature and composition of the Gibbs free energy derivative, $\partial^2 G/\partial\phi^2$, which provides the thermodynamic driving force for phase separation if dependent on preparation technique would lead to the preparation-dependent relative growth rates.

The growth rates $R(q)$ should have a quadratic dependence on q^2 as shown in Eq. (9) but in practice, the curvature is much flatter than this as has been frequently reported in the literature. Non instantaneous temperature jumps have been suggested as a possible cause of such flat $R(q)$ curves [36].

7.4. The maximum scattering wave number (q_m)

The wave numbers of maximum growth rate, q_m obtained from both preparation methods appear to be virtually independent of temperature (i.e. of quench depth) as seen in Fig. 7. The apparent non-dependence of q_m on quench depth has been reported for other systems [37]. It may result from the fact that to reach the deeper quenches the sample passes through a long region of instability, and that the initial

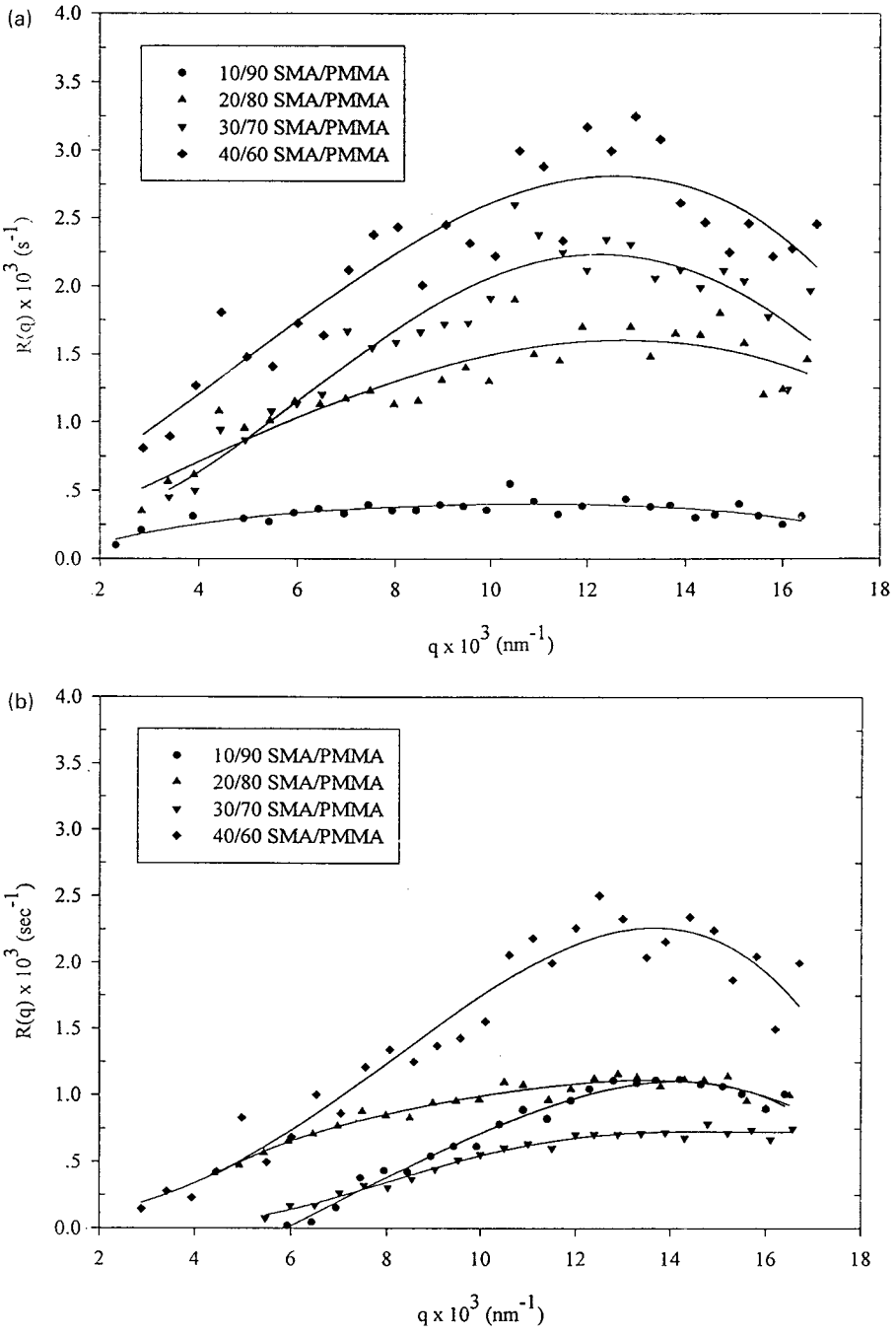

Fig. 6. Plots of $R(q)$ against q for blends which were isothermally heated at different temperatures: (a) solution cast blends, (b) melt mixed blends. ($T_{jump} = 210$°C for 20/80, 30/70 and 40/60 SMA/PMMAe blends; $T_{jump} = 220$°C for 10/90 SMA/PMMAe blends).

phase separation domain size simply reflects an early stage in this passage. On the other hand values of q_m from the melt mixing method are somewhat lower than from the solution casting method as clearly shown in Fig. 7. This would then reflect the differences in the thermodynamic behaviour close to the spinodal already suggested in the previous section.

Since the values of q_m in melt mixed blends are very high, there is a question concerning phase separation outside the q-range of the experiment. This is related to the delay time behaviour, which will be presented later on. As already mentioned X-ray or neutron scattering, with their shorter wavelengths, would be desirable techniques to explore this possibility, however there are problems with applying either technique to this blend. X-ray scattering relies on the electron density differences between the different compositions developing in phase separation. For the two polymers here, the differences are very small, making early stages difficult to detect. Preliminary small angle X-ray experiment on samples quenched during the delay times could detect no changes from the as-made samples. This may mean either

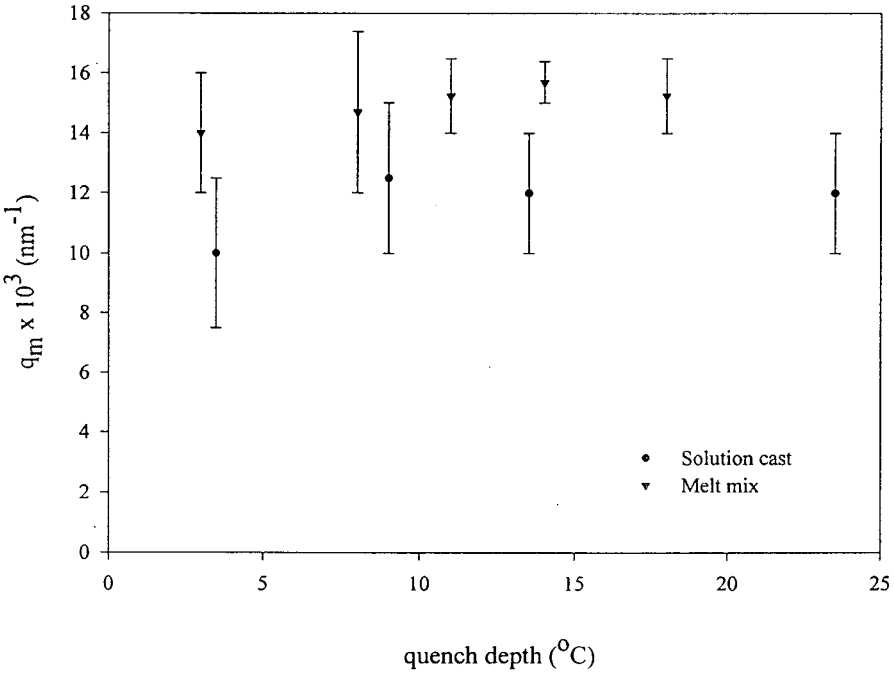

Fig. 7. Plots of q_m against quench depth for SMA/PMMAe (30/70) blends, prepared by solution casting and melt mixing methods.

nothing has occurred or that the signals are too weak. In small angle neutron scattering the differences between the compositions can be greatly enhanced by deuterating one polymer. Unfortunately for this system this raises the temperature of the phase boundary and means that sample degradation again becomes a serious problem. We shall be exploring means of overcoming these difficulties, and of using spectroscopic techniques in order to answer the questions about the initial phase size raised by the delay times observed.

7.5. The maximum growth rate ($R(q_m)$)

Fig. 8 depicts the change of $\sqrt{R(q_m)}$ with temperature, and, as can be seen $\sqrt{R(q_m)}$ increases linearly with quench depth, i.e. phase separation proceeds faster with increasing temperature. This is in contrast to the behaviour of q_m described in the previous section, and implies that, if q_m may reflect what happens at the instant of passing throughout the spinodal (or at least very soon afterwards), $R(q)$ is determined much more

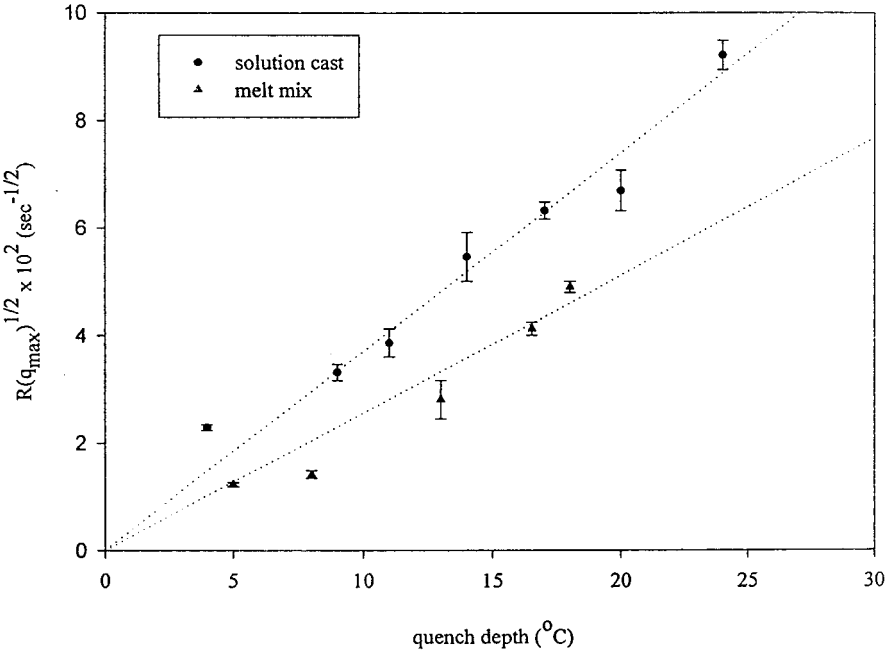

Fig. 8. Effects of preparation method on $R(q_m)$ for SMA/PMMAe (40/60) blends. As seen in this figure, $R(q_m)^{1/2}$ increases linearly with quench depth.

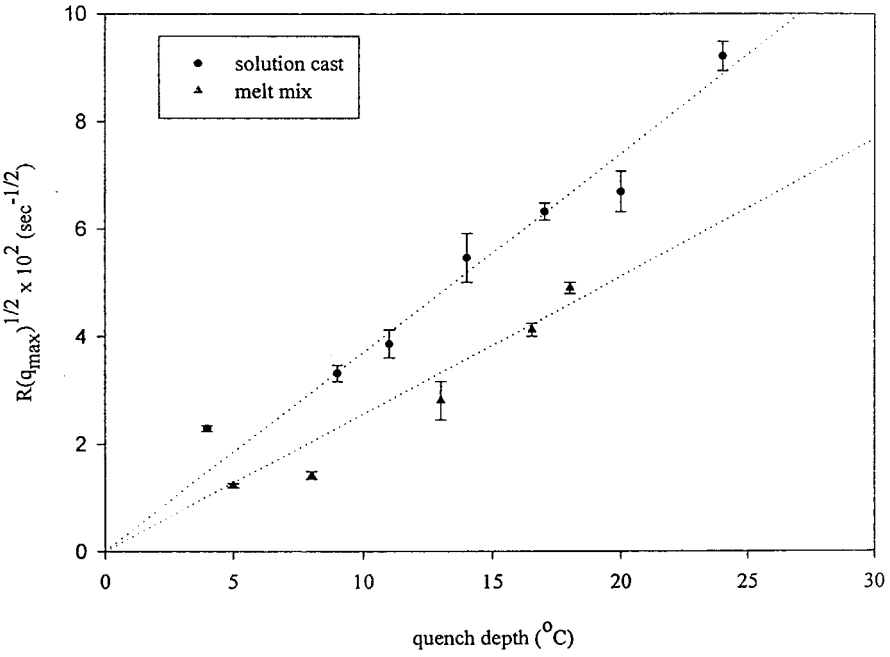

Fig. 9. A typical plot of intensity against time and q for melt mixed SMA/PMMAe (40/60) blends, obtained from a temperature jump experiment at 210°C.

closely by the final temperature at which the phase separation develops. By inserting the usual $\chi \propto 1/T$ variation into Eq. (12) we obtain

$$R(q_m)^{1/2} \propto (T - T_s) \tag{24}$$

Fig. 8 shows that $R(q_m)$ relates to square of the quench depth and in this respect the C–H prediction is obeyed by the data.

Considering the same quench depth, the solution cast blends appear to show higher maximum growth rates than the melt mixed ones which is not as would be expected from the relative positions of the phase boundaries, and would again imply differences in the thermodynamic behaviour.

7.6. Delay time (τ_d)

According to the Cahn–Hilliard theory, the phase separation via spinodal decomposition should occur spontaneously and immediately after heating into the phase separation regime. Surprisingly, it was found that a delay time frequently appears at the beginning of phase separation (shown in Fig. 2). Caution should be shown in interpreting these delays in terms of physical behaviour because there are a number of potential limitations in the technique which may show up as artefacts such as a delay times. We are confident that the response time of the apparatus is not a problem given the length of the delays shown in Fig. 9. On the other hand it is more difficult to rule out a lack of sensitivity to the refractive index difference in the very early stages or a phase separation outside the q-range accessible by light scattering. As discussed in Section 4, X-ray or neutron scattering would help answer this question but both have serious experimental difficulties for this blend. There is internal evidence in the data that may convince us we are truly in the early stages of spinodal decomposition after the delay time. Intensities increase exponentially after the delay time as expected from the linearised theory, and this suggests that the intensities do still fall in the early stages. The peak first grows at fixed angle and then shifts toward the low wave vector as would be expected for spinodal decomposition (shown in Fig. 9). The initial high intensities at low q are probably due to impurities in the blends and the transmitted light near the beam stop.

Fig. 10 shows the variation of the delay times with the quench depth for all the samples. As quench depth decreases, the delay time increases substantially. This, we believe, is due to the reduction in phase separation driving force as quench depth decreases. There are small differences between the values for samples prepared by the two methods. It appears that delay time is inversely related to $R(q)$ — i.e. those which have high $R(q)$, have low delay time.

If we assume for now that the delay times have a physical cause and are not artefacts, then we can examine the possible cause in terms of the effects of entanglements. As shown in Eqs. (21) and (22), it can be seen that the $\tau_d R(q)$ values can be used to distinguish whether A–B or A–A entanglement networks are appropriate for this system. For A–B entanglements, the product of delay time and growth rate should be independent of q, whereas in the case of A–A entanglements $\tau_d R(q)$ depends on q. $\tau_d R(q)$ was plotted against q for both solution cast and melt mixing methods as shown in Fig. 11. It was found that $\tau_d R(q)$ apparently depends on sample preparation method; solution cast blends show higher $\tau_d R(q)$ values than those of melt

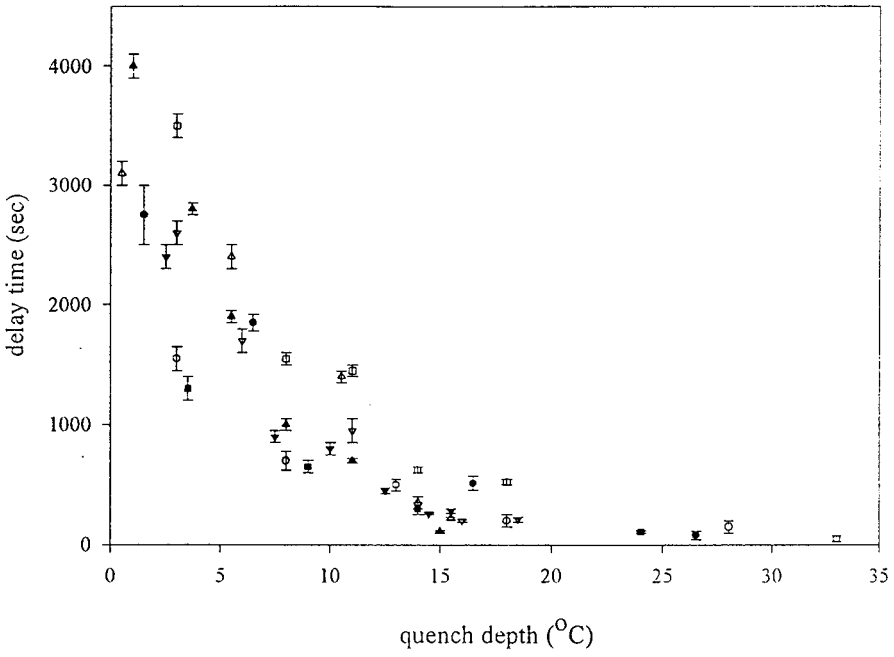

Fig. 10. Plots of delay time against quench depth for SMA/PMMAe blends (●: 10/90; ▲: 20/80; ■: 30/70; ▼: 40/60). Filled objects represent solution cast blends, unfilled objects represent melt mixed blends.

mixed one. In Fig. 11 we also plot the variation with q of Eq. (22) using upper and lower limits of N_e. We have used $b = 0.22$ nm. [38] and $N = 1200$. Not only is it clear that the experimental q-variation is very much less than predicted, but the values of N_e required to fit the data are nonsense, being of order unity or less! On the other hand if we assume there is effectively no q-variation and use Eq. (21) to obtain values of N_e from the average values of $\tau_d R(q)$ in Fig. 11 we also obtain

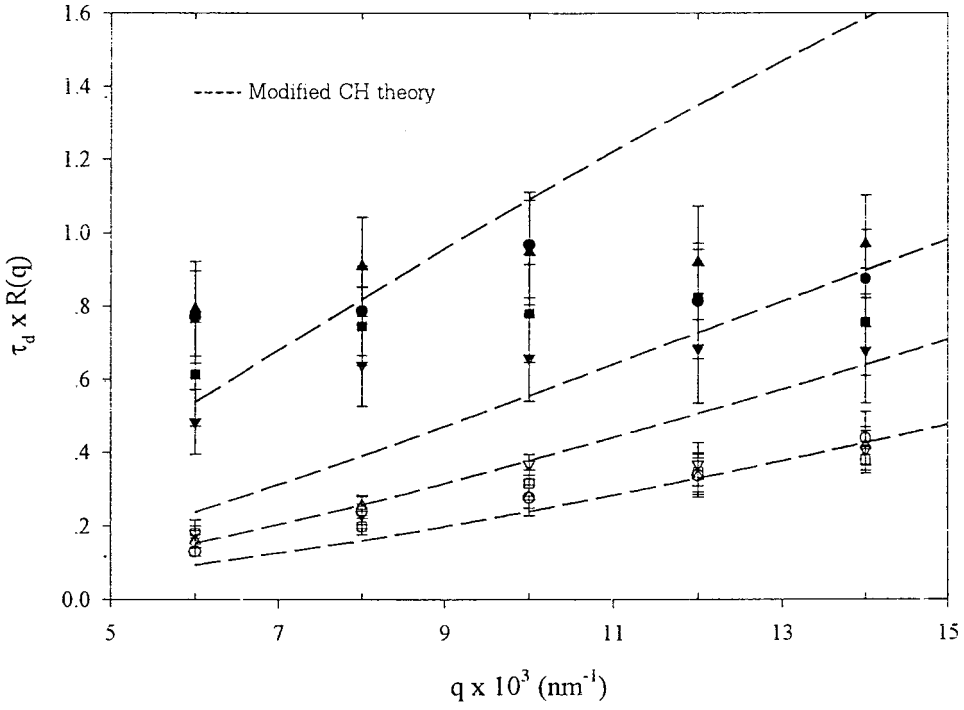

Fig. 11. Plots of $\tau_d \times R(q)$ against q for 30/70 SMA/PMMAe blends. (●, $T_{jump} = 200$°C, solution cast blend; ▲, $T_{jump} = 205.5$°C, solution cast blend; ▼, $T_{jump} = 210.5$°C, solution cast blend; ■, $T_{jump} = 220$°C, solution cast blend; ○, $T_{jump} = 195$°C, melt mixed blend; △, $T_{jump} = 200$°C, melt mixed blend; ▽, $T_{jump} = 206$°C, melt mixed blend; □, $T_{jump} = 210$°C, melt mixed blend).

nonsensical values of order N! There is clearly a serious problem here which may be due to experimental limitations or to approximations in the theory. In particular if for some reasons the rheological relaxation time is very long due to some long lived specific interactions, the assumptions which lead to Eq. (13), which is an approximation to Eq. (13) of Ref. [18] may become invalid, and the subsequent development breaks down. In order to utilise the exact expressions, detailed knowledge of the rheological response of the blend is required. Until further experiments can be made exploring the q-range outside those reported here, during the delay times, as suggested earlier in Section 4, it will not be possible to resolve these questions.

8. Conclusions

The results reported here show clear influences of sample preparation methods on phase behaviour, i.e. spinodal and cloud point curves of melt mixed samples were lower than those of solution cast blends. The Gordon–Taylor–Kwei equation, which accounts for the effect of interactions between polymers, shows good agreement with the glass transition temperature data confirming the existence of specific interactions in this blend. It is suggested that the stronger intermolecular interactions facilitated in solution cast blends by the more intimate mixing might play a crucial role in producing the differences arising from sample preparation method. Temperature jump experiments showed that sample preparation also affects the kinetics of phase separation. The Cahn–Hilliard growth rates $R(q)$ vary in a complex way depending on concentration and sample preparation. Delay time behaviour was investigated closely. It was found that sample preparation, composition, temperature, and q all affect the delay time. The values of $\tau_d R(q)$ appear to depend on preparation methods. Comparison of the observed delay times with the predictions of viscoelastic theory show serious contradictions which may indicate the origin of the apparent delays lies elsewhere in this case.

Acknowledgements

We would like to thank the National Science and Technology Development Agency of Thailand, and the British Council (Thailand) for their financial support.

References

[1] Shaw MT. J Appl Polym Sci 1974;18:449–72.
[2] Reich S, Cohen Y. J Polym Sci, Part B: Polym Phys 1981;19:1255–67.
[3] Varnell DF, Runt JP, Coleman MM. Macromolecules 1981;14:1350–6.
[4] Inoue T, Ougizawa T, Yasuda O, Miyasaka K. Macromolecules 1985;18:57–63.
[5] Saldanha JM, Kyu T. Macromolecules 1987;20:2840–7.
[6] Nishimoto M, Keskkula H, Paul DR. Polymer 1991;32:272–8.
[7] Neo MK, Gho SH. Polymer 1992;33:2012–4.
[8] Woo EM, Chean CS. Polymer 1996;37:4111–8.
[9] Gaurab D, Banerjee AN. J Appl Polym Sci 1996;61:1473–8.
[10] Robard A, Patterson D. Macromolecules 1977;10:706–8.
[11] Thongyai S. PhD Thesis, Imperial College, London, 1994.
[12] Manda D. PhD Thesis, Imperial College, London, 1998.
[13] Manda D, Higgins JS, Aelmans NJ, Reid VMC. Submitted for publication.
[14] Brannock GR, Barlow JW, Paul DR. J Polym Sci, Part B: Polym Phys 1991;29:413–29.
[15] Feng H, Shen L, Feng Z. Eur Polym J 1995;31:243–7.
[16] Aelmans NJ, Reid VMC, Higgins JS. Polymer 1999;40:5051–62.
[17] Chopra D, Vlassopoulos D, Hatzikiriakos SG. J Rheol 1998;42:1227–47.
[18] Bank M, Leffingwell J, Thies C. J Polym Sci, Part A-2 1972;10:1097–109.
[19] Binder K, Frisch HL, Jackle J. J Chem Phys 1986;85:1505–12.
[20] Clarke N, Mcleish TCB, Pavawongsak S, Higgins JS. Macromolecules 1997;30:4459–63.
[21] Gerard H, Higgins JS, Clarke N. Macromolecules 1999;32:5411–22.
[22] Flory P. Principles of polymer chemistry. Ithaca, NY: Cornell University Press, 1971 (chap. 12).
[23] de Gennes PG. J Chem Phys 1980;72:4756–63.
[24] Clarke N. PhD Thesis, University of Sheffield, 1994.
[25] Doi M, Edwards SF. The theory of polymer dynamics. New York: Oxford University Press, 1986 (chap. 7).
[26] Bauruah SD, Laskar NC. J Appl Polym Sci 1996;60:649–56.
[27] Wang FC. J Chromatogr, A 1997;765:279–85.
[28] Klumperman B, O'Driscoll KF. Polymer 1993;34:1032–7.
[29] Tacx JCJF, Meijerink NLJ, Suen K. Polymer 1996;37:4307–10.
[30] Guo W, Higgins JS. Polymer 1990;31:699–706.
[31] Pavawongsak S. PhD Thesis, Imperial College, London, 1996.
[32] Cook HE. Acta Metall 1970;18:297–306.
[33] Coleman ME, Graf JF, Painter PC. Specific interactions and the miscibility of polymer blends. Technomic Publishing Company, 1991.
[34] Fox TG. Bull Am Phys Soc 1956;1(3):123.
[35] Gordon M, Taylor JS. J Appl Chem 1952;2:493–500.
[36] Carmesin HO, Heermann DW, Binder K. Phys B-Condens Matter 1986;65:89–102.
[37] Higgins JS, Fruitwala H, Tomlins PE. Macromolecules 1989;22:3674–81.
[38] Brandrup J, Immergut EH. Polymer handbook, vol. 1. New York: Wiley, 1992. p. 989.